Journal of Hazardous Materials 496 (2025) 139289

Contents lists available at ScienceDirect

Journal of Hazardous Materials

journal homepage: www.elsevier.com/locate/jhazmat

The return of natural lead to the Northeast Atlantic Ocean captured by brown algae

Carme Pacín [a,b,*], Jesús R. Aboal [a], J. Ángel Fernández [a], Antón Vázquez-Arias [a], Adéla Šípková [c], Michael Komárek [c], Vladislav Chrastný [c]

[a] CRETUS Center, Department of Functional Biology, Ecology Unit, Universidade de Santiago de Compostela, Santiago de Compostela 15782, Spain
[b] CIQUS Center, Department of Physical Chemistry, Universidade de Santiago de Compostela, Santiago de Compostela 15782, Spain
[c] Department of Environmental Geosciences, Faculty of Environmental Sciences, Czech University of Life Sciences Prague, Kamýcká 129, Prague-Suchdol 16500, Czech Republic

HIGHLIGHTS

- Long-term Pb isotope data reveal 30-year pollution trends in brown algae.
- Isotopic shifts show declining anthropogenic Pb contamination since 1990.
- Pb concentrations in *Fucus* spp. remained stable despite regulatory actions.
- Stable Pb levels likely reflect increased bioavailability and sediment influence.
- This study establishes a robust isotopic baseline for a region with scarce data.

GRAPHICAL ABSTRACT

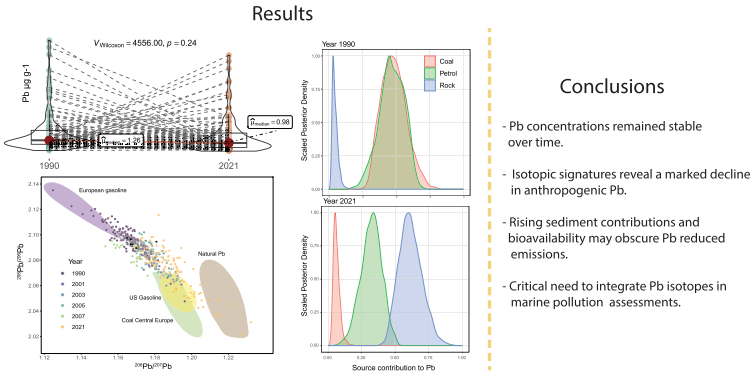

ARTICLE INFO

Keywords:
Stable isotopes
Heavy metal
Potentially Toxic Elements
Temporal trend
Pollution
Biomonitoring
Seaweed

ABSTRACT

Lead (Pb) is a highly toxic pollutant with serious ecological implications. This study investigates 30-year trends (1990–2021) in Pb concentrations and isotopic signatures ($^{206}Pb/^{207}Pb$ and $^{208}Pb/^{206}Pb$) in the brown algae *Fucus* spp. from the Northeast Atlantic Ocean (n = 446). Pb concentrations showed only modest, non-significant 21.9 % decline. In contrast, isotopic data revealed a clear shift from anthropogenic to natural sources. Bayesian mixing models (MixSIAR) supported this trend, indicating an increase in natural contributions, rising from 4.7 % in 1990 to 61.5 % in 2021, mirroring reductions in coal combustion (from 48.4 % to 6.3 %) and petrol-related sources (from 46.9 % to 32.2 %). This divergence between concentrations and isotopic trends likely reflects a substantial increase in sediment-derived Pb (189.3 % in 2021 compared to 13–49 % during 1990–2007), as well as enhanced bioavailability driven by environmental changes such as ocean acidification. Elevated Pb levels were found in inner estuarine zones dominated by *Fucus ceranoides*, but no latitudinal pattern or isotopic differences among species were observed. Overall, the findings highlight the complex dynamics of Pb in coastal ecosystems and the limitations of relying solely on concentration data to assess pollution trends. Isotope analyses have

* Corresponding author at: CRETUS Center, Department of Functional Biology, Ecology Unit, Universidade de Santiago de Compostela, Santiago de Compostela 15782, Spain.
E-mail address: mcarme.pacin@usc.es (C. Pacín).

https://doi.org/10.1016/j.jhazmat.2025.139289
Received 10 March 2025; Received in revised form 9 July 2025; Accepted 15 July 2025
Available online 17 July 2025

proven essential for source attribution, revealing a progressive shift toward natural Pb sources and supporting the effectiveness of regulatory measures such as the global phase-out of leaded gasoline. However, the study underscores that increased Pb bioavailability, driven by acidification and other global environmental changes, may offset the benefits of reduced emissions. Finally, this work provides a valuable isotopic baseline for a region where such data remain scarce, supporting future environmental monitoring and source-tracing efforts.

1. Introduction

Lead is one of the most toxic elements, with no known metabolic function in organisms and adverse effects even at trace levels [1,2]. While the natural weathering of Earth's crust can contribute to environmental Pb levels [3], its widespread prevalence in the environment today is largely a consequence of anthropogenic activities, including mining, industrial processes, and the historical use of leaded gasoline [4,5]. Emissions peaked in the 20th century but declined after the phase-out of leaded gasoline from the 1990s onwards [6]. However, certain sources persist, such as cement production, battery manufacturing, ceramics, mining, and residual Pb in fuels [7–9].

Coastal ecosystems are particularly vulnerable to Pb pollution as they act as sinks for terrestrial sources of contamination due to their proximity to land-based inputs [10–12]. In these environments, Pb can be found in sediment particles, dissolved in the water, or concentrated by the biota, including intertidal seaweeds of the genus *Fucus*. These foundational species are vital in North Atlantic coastal ecosystems as habitat engineers and primary producers in dynamic intertidal zones [13,14]. However, their ability to accumulate Pb and other potentially toxic elements [15–17] raises ecological concerns.

Beyond their environmental impact, the capacity of brown algae to bioconcentrate contaminants also enables their use as biomonitors of coastal pollution. This characteristic has led to their widespread application in monitoring pollutants such as Pb. Traditional assessments of Pb pollution that rely on measuring total Pb concentrations, while informative, do not identify pollution sources. In contrast, the Pb isotopic ratios $^{206}Pb/^{207}Pb$ and $^{208}Pb/^{206}Pb$, act as unique chemical signatures [18], enabling the identification and tracking of contamination sources [19–22]. Unlike for other elements (e.g. N, C, Hg, etc.) [23], metabolic and biogeochemical processes display no isotopic discrimination for Pb, so these dynamics do not affect Pb isotopic ratios. Therefore, analyzing the isotopic signature of Pb accumulated on seaweeds can provide valuable information on marine pollution sources, informing on contamination pathways and ecological impacts. However, research on marine organisms, particularly seaweeds, remains scarce [24–26]. Moreover, because environmental fractionation does not occur for Pb, the use of a temporal series of samples can provide information on the evolution of pollution sources over time, helping us understand the effectiveness of environmental regulations. However, to date only a few studies have evaluated temporal trends of Pb isotopic ratios in marine biota, all with a limited sample size [27–31], highlighting the need to better understand how contamination sources and environmental responses evolve over time in marine environments.

This study addresses the scarcity of temporal data in marine organisms by making use of a high-resolution, multi-decadal dataset with broad spatial coverage and a robust number of samples. Specifically, we analyzed samples from the Galician Environmental Specimens Bank, which contains over three decades of coastal monitoring data. The dataset comprises 446 samples of *Fucus ceranoides*, *F. spiralis*, and *F. vesiculosus* collected between 1989 and 2021 from 173 stations along the NW Spanish coast. This region represents a microcosm of broader environmental challenges in the Northern Hemisphere, characterized by a densely populated coastline, intense industrial activity, high maritime traffic, and strict environmental regulations like other European nations. By analyzing total Pb concentrations and isotopic compositions, this study aims to: (1) assess temporal trends in Pb pollution; (2) identify the origin of Pb contamination impacting *Fucus* spp. and their ecosystem over the past 30 years; and (3) evaluate spatial and species-specific patterns in Pb accumulation and isotopic ratios. The hypothesis to be tested is that Pb concentrations and isotopic ratios in *Fucus* spp. have remained stable over time, with no significant spatial, or species-specific variation.

2. Material and methods

2.1. Survey area

The study was conducted in the northwest of Spain (Galicia region). This region boasts a 1498 km coastline along the Atlantic Ocean and the Bay of Biscay (approximately 25 % of the Iberian Peninsula), characterized by unique coastal inlets known as rias, formed by the submergence of river valleys due to land subsidence (see Fig. 1). Galicia's oceanic climate is mild, with abundant precipitation [32]. In addition, the geological diversity of the region includes mainly granite, but also schists, slates, basic and ultrabasic rocks, limestone, and quartzites, each with variable Pb content [33].

In the last decades, Galicia's coastline has supported major industries such as automotive manufacturing, shipbuilding, energy production, wood industry, ferrous and non-ferrous metallurgy, and dense human populations [34]. As in most European countries, Spain banned leaded gasoline in 2001 [6].

2.2. Sample collection

Sampling campaigns were conducted during low tide in July of 1989–1990 (hereafter referred to as 1990), 2001, 2003, 2005, 2007, and 2021. A total of 173 sites were sampled leading to the collection of 446 samples of the brown algae *Fucus ceranoides, F. vesiculosus,* and *F. spiralis* (Fig. 1). At each site, a composite sample (n = 30 thalli), was obtained to account for intra-site variability along a 50-meter transect in a zigzag pattern. The algae were cleaned on-site with seawater, in order to remove sediment particles and epiphytes, according to the most recent recommendations [35], and transported to the laboratory in a cooler. Detailed protocols for sampling, washing, and processing can be consulted in the Supporting Information [35].

With few exceptions, samples collected in 1990 were also taken from the same sites in 2021. Similarly, samples gathered in 2001 were collected again at the same sites in 2003, 2005, 2007, and 2021. Sampling sites were distributed along the entire coastline of the study area, covering open sea zones, estuaries, areas impacted by anthropogenic activities (e.g., industries, urban developments), and regions without known pollution sources. The selection included both protected areas, such as national parks and sites within the Natura 2000 network, and historically impacted areas, such as the ria O Burgo (ria d in Fig. 1), once considered the most contaminated estuary in Europe. This comprehensive site selection allows for an accurate representation of the overall regional pattern of coastal pollution.

Fucus ceranoides is restricted to brackish inner rias, while *F. spiralis* and *F. vesiculosus* are found in more exposed, ocean-influenced areas, where they often coexist and hybridize [36]. Although *F. vesiculosus* is generally distinguished by air bladders, these structures are not always present, which complicates field identification. Recent studies have further introduced taxonomic uncertainty by dividing *F. spiralis* into *F. spiralis* and *F. macroguiryi* [37]. To address these taxonomic uncertainties and identification challenges, *F. spiralis* and *F. vesiculosus*

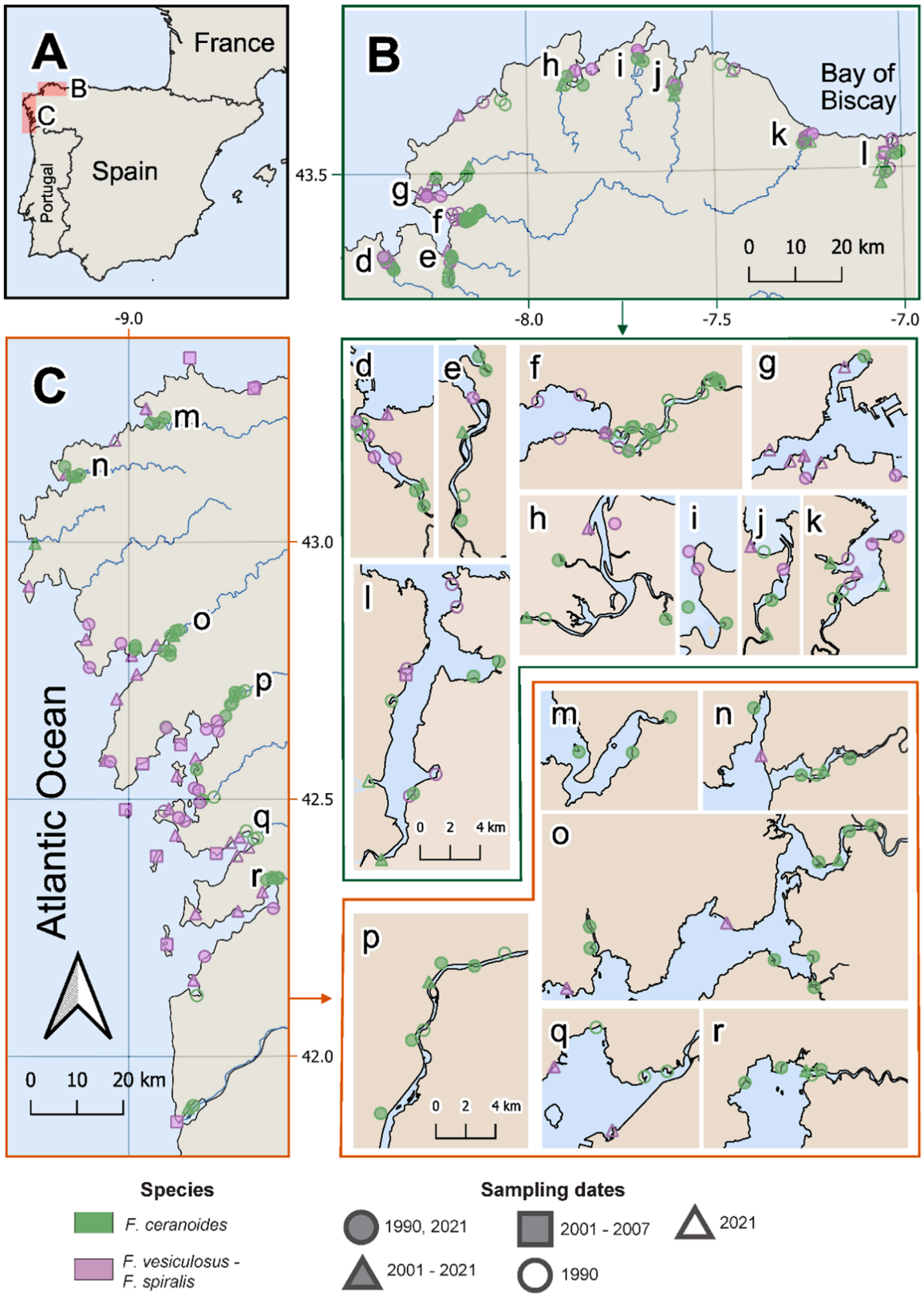

Fig. 1. Map of the study area. Panels A-C display an overview of the region, with B and C showing the sampling sites (sites). Panels d-l and m-r present detailed maps of sites that are densely clustered and difficult to distinguish in B and C, respectively. Different colors represent the species sampled (*F. ceranoides* and *F. vesiculosus–F. spiralis*) while distinct symbols indicate the sampling periods: 1990–2021, 2001–2021, and 2001–2007, or those sampled exclusively in 1990 or 2021. To reduce clutter, incomplete samplings from 2001, 2003, 2005, and 2007 are grouped under the 2001–2007 symbol.

Table 1
Isotopic signatures of reference materials from this study and compiled from the literature. Reported values correspond to $^{206}Pb/^{207}Pb$ and $^{208}Pb/^{206}Pb$ ratios. Sources selected for the MixSIAR model (coal, unleaded petrol and diesel, leaded petrol, and rock) are indicated with "(MixSIAR)" in parentheses. Pb concentrations of the sediments analyzed in this study are provided in Table S2.

		$^{206}Pb/^{207}Pb$	$^{208}Pb/^{206}Pb$	Reference
Coal	**La Jagua (Columbia)**	1.219	2.077	Farmer et al., 1999 [53]
(MixSIAR)	**Study area (As Pontes)**	1.130	2.017	Díaz-Somoano et al., 2007 [54]
	Study area (Meirama)	1.183	2.019	Díaz-Somoano et al., 2007 [54]
	Median European Coal	1.185	2.079	Díaz-Somoano et al., 2009 [55]
	Indonesia	1.184	2.093	Díaz-Somoano et al., 2009 [55]
	Powder River Basin (US)	1.224	2.032	Whang et al., 2019 [56]
	Tarragona (Spain)	1.185	2.075	Plasencia et al., 2025 [57,58]
	Mean	1.187	2.056	-
	sd	0.031	0.032	-
Unleaded Petrol	**Gasoline Study Area**	1.160	2.104	This study
(MixSIAR)	**Diesel Study Area**	1.166	2.095	This study
	France	1.131	2.128	Cloquet et al., 2006 [57]
	Gasoline Greenland	1.160	2.060	Astray et al., 2024 [19]
	Gasoline Norway	1.148	2.124	Chrastný et al., 2018 [9]
	Diesel Norway	1.153	2.129	Chrastný et al., 2018 [9]
	Diesel Tarragona (Spain)	1.132	2.134	Plasencia et al., 2025 [58]
	Gasoline Tarragona (Spain)	1.161	2.104	Plasencia et al., 2025 [58]
	Mean	1.151	2.110	
	sd	0.013	0.025	
Leaded Petrol	**Gasoline France**	1.083	-	Véron et al., 1999 [59]
(MixSIAR)	**Gasoline France**	1.084		Monna et al., 1997 [60]
	Gasoline Switzerland	1.113	2.144	Chiaradia & Cupelin, 2000 [61]
	Gasoline Czech Republic	1.040	2.221	Novak et al., 2003 [62]
	Mean	1.086	2.182	
	sd	0.029	0.038	
Rocks (Study area, MixSIAR)	**calc-alkaline granite Viveiro**	1.228	1.990	This study
	calc-alkaline granite O Pindo	1.211	2.030	This study
	two-micas alkaline granite Vilarseco	1.305	1.865	This study
	Peridotite (Dunite) Ortigueira	1.219	2.076	This study
	Pizarra Viveiro	1.209	2.070	This study
	Schist Ordes	1.243	2.022	This study
	Mean	1.236	2.009	
	sd	0.036	0.077	
Sediments	**S1, 1990**	1.227	2.036	This study
(Study área)	**S2, 1990**	1.170	2.094	This study
	S3, 2007	1.181	2.095	This study
	S4, 2001	1.170	2.090	This study
	S5, 2005	1.168	2.093	This study
	S6, 2007	1.194	2.072	This study
	S7, 2001	1.165	2.098	This study
	S8, 2005	1.167	2.093	This study
	S9, 2003	1.175	2.089	This study
	S10, 1990	1.167	2.097	This study
	S11, 1990	1.169	2.101	This study
	S12, 2021	1.189	2.074	This study
	S13, 2021	1.175	2.092	This study
	S14, 2021	1.188	2.070	This study
	S15, 2021	1.181	2.098	This study
	S16, 2021	1.170	2.095	This study
	S17, 2021	1.166	2.102	This study
	S18, 2021	1.175	2.089	This study
	S19, 2021	1.171	2.097	This study
	S20, 2021	1.175	2.091	This study
Upper continental crust		1.205	2.06	Kylander et al., 2005 [63]
Ores	**Study Area**	1.146	2.125	Tornos & Arias, 1993 [64]
	Study Area	1.144	2.127	Tornos et al., 1996 [65]
	Study Area	1.147	2.123	Arias, 1989 [66]
	North Portugal	1.169	2.097	Neiva et al., 2008 [67]
	Study area	1.165	2.103	Millos et al., 2014 [68]
Ceramic industry	**Arcade (Study area)**	1.189	2.073	This study
Waste incineration	**Switzerland**	1.151	2.108	Hansmann & Köppel., 2000 [69]
	France	1.154	2.107	Carignan et al., 2005 [70]
	Tarragona (Spain)	1.162	2.101	Plasencia et al., 2025 [58]
	France	1.149	-	Monna et al., 1997 [60]
E-waste	**México**	1.190	2.053	Río-Salas et al., 2025 [71]
	East Antartica	1.150	2.117	Townsend et al., 2009 [72]
	Shantou (China)	1.152	2.109	Jiang et al., 2019 [73]
Aerosols	**Prepollution (Study area)**	1.255	-	Kylander et al., 2005 [74]
	Sahara dust	1.209	2.062	Schleicher et al., 2020 [75]
	Spain aerosol	1.109	2.149	Bollhöfer & Rosman, 2001 [76]
	Morocco and Senegal	1.159	2.104	Zhang et al., 2024 [77]

(*continued on next page*)

Table 1 (*continued*)

		$^{206}Pb/^{207}Pb$	$^{208}Pb/^{206}Pb$	Reference
Seawater	**NE Atlantic Ocean**	1.1815	2.059	Véron et al., 1994 [78]
	NE Atlantic Ocean	1.173	2.082	Pinedo-González et al., 2018 [79]
	NE Atlantic Ocean	1.184	2. 069	Zurbrick et al., 2018 [80]
Mussel	**France**	1.167	2.0887	Couture et al., 2010[30]
	France	~1.170	~2.095	Barreira et al., 2025 [31]
Seaweed	***Fucus* spp., Greenland**	1.138	2.120	Søndergaard et al., 2010[27]
	***Iridaea cordata*, East Antartica**	1.086	2.170	Runcie et al., 2009 [25]

were combined for analysis in this study, so we refer to them as *F. vesiculosus – F. spiralis*, while *F. ceranoides* was examined separately.

2.3. Sample preparation and analysis

The apical parts of each thallus corresponding to the three apical dichotomies and representing the last growth period [35] were selected. Samples with reproductive structures, apparent damage, or epiphytes were excluded. Selected thalli were dried in a forced-air oven at 40ºC until constant weight and then homogenized using a tangential mixer mill with zirconium oxide grinding vessels (Retsch MM400). Homogenized samples were stored in hermetically sealed glass containers, at room temperature, protected from light in the Galician Environmental Specimen Bank [38] until chemical analysis.

Before analysis, 0.3 g of the samples were re-dried at 100°C and digested with 69 % (w/w) HNO_3 in a Milestone Ultrawave. Pb isotopic compositions were determined using a Thermo Scientific™ iCAP™ Q ICP-MS (Inductively Coupled Plasma Mass Spectrometer) at the Czech University of Life Sciences, Prague. Pb concentrations were determined with an Agilent 7700x ICP-MS at the Research Support Services Unit of the Universidade de Santiago de Compostela.

2.4. Representative materials

Representative materials were selected to represent potential sources of Pb contamination and characterize the range of Pb isotopic signatures in the study area (Table 1). Sediment samples from 1990, 2001, 2003, 2005, 2007 and 2021 were collected concurrently with the algal samples in their immediate vicinity using a spatula, taking the top 5 mm of the sediment layer to capture recent deposition. Following collection, samples were sieved through a 200 nm mesh and dried prior to chemical analysis. Other representative materials, collected in 2023, included representative geological materials (calc-alkaline granite, two-mica alkaline granite, peridotite, slate, and schist), local ceramics with high Pb content, and gasoline and diesel from a local refinery. Isotopic compositions and Pb concentrations for the reference materials were determined following the same protocols applied to the algal samples.

2.5. Quality control

Quality control measures for Pb concentration analysis included analytical blanks, sample replicates, and certified reference material (*Fucus vesiculosus* ERM-CD200) analyzed at a frequency of one per 30 samples. The Percent Relative Difference was 3.7 %, with a recovery rate of 93.2 %.

The procedural blanks exhibited Pb concentrations ranging between 0.035 and 0.138 μg L^{-1}, with a limit of quantification (LOQ) of 0.73 μg L^{-1}, corresponding to approximately 0.12 μg g^{-1} in the solid samples. This LOQ was exceeded in all samples except one. For isotopic ratios, each sample was analyzed in 10 replicate scans, with an integration time of 60 ms per isotope (^{206}Pb, ^{207}Pb, and ^{208}Pb). Lead concentrations in solution ranged between 0.2–2 μg L^{-1}. The relative standard deviation (RSD) for isotope ratios was below 0.2 % for individual sample runs; otherwise, the instrument was recalibrated before proceeding. The replicates showed Percent Relative Difference of 0.42 % for $^{206/207}Pb$ and 0.50 % for $^{208}Pb/^{206}Pb$. Importantly, these replicate values correspond to the same sample analyzed across different analytical sessions (i.e., on different days). NIST SRM 981 was analyzed as an isotopic standard every two samples, with each sample corrected using the most recent standard measurement (sample-standard bracketing approach). Raw isotope ratios were corrected using empirically derived normalization factors (1.0933 for $^{206}Pb/^{207}Pb$ and 2.168 for $^{208}Pb/^{206}Pb$) that account for the instrument's mass bias characteristics. The measured ratios of NIST SRM 981 showed excellent agreement with reference values, with median deviations of + 0.28 % for $^{206}Pb/^{207}Pb$ (median measured: 1.0964 vs reference: 1.0933) and −0.64 % for $^{208}Pb/^{206}Pb$ (median measured: 2.1542 vs reference: 2.168). The high recovery rates (100.28 % and 99.36 %, respectively) and low median relative standard deviations (RSD < 0.33 % for both ratios) demonstrate both the accuracy and precision of our measurements [39].

Isotopic ratios were verified against NIST SRM 1573a (tomato leaves), NIST SRM 1515 (apple leaves), and IAEA-336 (epiphytic lichen). Measured values closely matched reported values (Table S1) [40–42].

Finally, to evaluate whether matrix components could limit the accuracy of isotopic measurements, we conducted additional tests using standard anion exchange chromatography on three thalli and three sediment samples. An aliquot of each sample was evaporated to dryness and re-dissolved in 0.5 M HNO_3 - 0.2 M HBr. The separation was carried out using a column containing 2 mL of AG1-X8 resin (100–200 mesh), which was first cleaned with demineralized water and equilibrated with 0.5 M HNO_3 - 0.2 M HBr. The sample was then loaded onto the column, and the matrix components were eluted. Lead was collected using 0.45 M HNO_3 - 0.03 M HBr, evaporated to dryness, re-dissolved in 2 % HNO_3, and subsequently analyzed by ICP-MS. The isotopic ratios obtained from the purified samples were then compared to those from the same samples analyzed without prior separation. Differences were minimal: 0.1 % for $^{206}Pb/^{207}Pb$ and −0.01 % for $^{208}Pb/^{206}Pb$. These results indicate that matrix effects were negligible under our analytical conditions, and incomplete purification did not significantly affect the accuracy of isotopic measurements. Therefore, full separation was not applied systematically to all samples.

2.6. Data analysis

All statistical analyses were performed in R v4.4.1 [43] using the car, ggstatsplot, ggplot2, and MixSIAR packages [44–47]. Descriptive statistics and Shapiro-Wilk test were used to assess normality of Pb concentrations and isotopic ratios ($^{206}Pb/^{207}Pb$ and $^{208}Pb/^{206}Pb$). Due to significant deviations from normality, non-parametric methods were applied throughout. Differences in Pb and isotopic ratios between species and sampling years (n = 446) were tested using Kruskal-Wallis and Dunn's post hoc tests. Later, the dataset was restricted to only those sites that were resampled in different campaigns: the Wilcoxon signed-rank test compared concentrations in sites sampled in 1990 and 2021, and Friedman and Durbin-Conover post-hoc tests compared sites sampled in 2001 and revisited in 2003, 2005, 2007 and 2021. For years with co-occurring species at a given site, comparisons were made between each species across time. Pb/Fe ratios were also evaluated using the same approach. Spearman's rank correlations were used to examine relationships between Pb and Fe concentrations in algae, isotopic ratios in algae vs. sediments ($^{206}Pb/^{207}Pb$ and $^{208}Pb/^{206}Pb$), and between

$^{206}Pb/^{207}Pb$ and the inverse of Pb concentrations.

Spatial patterns were visualized using QGIS 3.36.3 [48], and Pb concentrations and isotopic ratio changes for each site across the study period were determined by comparing the earliest with the most recent available data points.

To estimate the proportional contributions of different Pb sources, a Bayesian isotopic mixing model was run using MixSIAR [47]. Source categories included Petrol (combined leaded/unleaded petrol and diesel), Coal, and Natural rock background. The initially disaggregated fuel sources exhibited strong posterior correlations in MixSIAR outputs (pairwise source correlation < –0.9), which indicated poor isotopic discrimination, justifying their aggregation into a single "Petrol-related sources" category. Different rock types representative of the study area's lithology (e.g., slates, schists, granites) were grouped into a single "natural source" end-member, as their Pb isotopic signatures showed substantial overlap. Sources such as e-waste or municipal waste incineration were excluded due to highly variable isotopic signatures and the lack of region-specific data. Coal isotope data from Colombia, Indonesia, and the U.S. were included to reflect the shift of the study area power plants toward imported coal in the early 2000s, ensuring realistic representation of the sources. Samples from 2001 to 2007 were grouped into a single temporal category after verifying consistent source contributions. The model was run with 3 chains of 300 000 iterations (burn-in = 150 000; thinning = 100) and showed excellent convergence (Gelman-Rubin < 1.05 for all parameters). Source signatures are detailed in Table 1.

To assess changes in Pb speciation over time, we used thermodynamic modeling with Visual MINTEQ [49] under representative seawater conditions for the study region. Regional acidification has been estimated at –0.0012 pH units per year, with surface seawater pH decreasing from approximately 8.10 to 8.06 between 1990 and 2021 [50]. Based on available data, we used a median Pb^{2+} concentration of 0.65 µg/L [51,52], and representative seawater temperatures of 15.36 °C for 1990 and 15.80 °C for 2021. We therefore modelled two scenarios: one representing baseline conditions (pH 8.10, 15.36 °C) and another representing 2021 conditions (pH 8.06, 15.80 °C). These simulations allowed us to estimate potential changes in Pb^{2+} speciation associated with ocean acidification and warming.

Sediment contributions to Pb concentrations were estimated using Fe as a geological tracer [81], with Pb and Fe ratios calculated from published sediment data for 1990, 2003, 2005, and 2007 [38,82], and supplemented by nine newly analyzed sediment samples from 2021. For each sampling site, sediment contributions were determined by pairing algal Pb concentrations with corresponding sediment data from the same year and site, using the following equation:

$$\text{sediment contribution} = \frac{\frac{[Pb]_{sediment}}{[Pb]_{algae}}}{\frac{[Fe]_{sediment}}{[Fe]_{algae}}} \quad (1)$$

The median sediment contribution was calculated for each year. Additionally, a Spearman correlation between Fe and Pb concentrations in algae was performed to further explore the potential sedimentary origin of Pb in the biota.

3. Results

Detailed Pb and Fe concentrations, isotopic ratios, site coordinates, and ria classifications for each site and Year of sampling for *Fucus* spp. and sediment samples are provided in Table S2.

3.1. Pb concentrations and temporal trends

Pb concentrations in *Fucus* ranged from 0.079 to 53.181 µg g^{-1} (dry weight), with a median of 1.1 µg g^{-1}. *F. ceranoides* showed significantly higher values (1.51 µg g^{-1}) than *F. vesiculosus–F. spiralis* (0.91 µg g^{-1}, $p = 4.46 \times 10^{-12}$), consistent with elevated levels where it predominantly occurs (Fig. 1, Fig. S1). No clear spatial gradient was detected, but localized hotspots, such as Ria do Burgo and Ria de Vigo (labeled d and r in Fig. S1, respectively), exhibited high concentrations.

Pb levels remained fairly stable over time, with slight recent declines. Kruskal-Wallis ($p = 3.45 \times 10^{-4}$) and post-hoc Dunn tests revealed differences between 1990–2003 ($p = 1.56 \times 10^{-3}$) and 2003–2007 ($p = 3.78 \times 10^{-3}$), but no consistent downward trend was detected. Site-specific analyses using Friedman ($p = 0.03$), Durbin-Conover, and Wilcoxon tests ($p = 0.24$) showed no significant variations among 2001, 2003, 2005, 2007, and 2021, and between 1990 and 2021, though 2021 consistently showed the lowest values (Fig. 2). At the individual site level, temporal patterns were mixed, with both increases and decreases and no consistent spatial trend. Median percent change across sites indicated a moderate decline of –21.87 % (Fig. S2). A similar pattern of stability was observed among the 50 samples showing the highest Pb concentrations. Lead and Fe concentrations in algae were strongly correlated (rho = 0.58, $p < 2.2 \times 10^{-16}$), suggesting the influence of the sediment. Additionally, using Fe as a lithogenic tracer [82], estimated sediment contributions to algal Pb were 43.5 % (1990), 46.3 % (2003), 49.3 % (2005), 13.0 % (2007), and 189.3 % (2021). The notably high value in 2021 (> 100 %) indicates a lower Pb concentration than expected based on sediment composition alone, while the opposite occurred for the rest of the years, and particularly for 2007. Accordingly, the Pb/Fe ratio in algae showed significant decreases over time, with 2021 values being notably lower than those of all other years ($p < 0.05$). Despite differences in sediment exposure, with *Fucus ceranoides* being more exposed than *F. vesiculosus–F. spiralis* due to its position within the rias, both groups exhibited similar temporal trends in Pb concentrations and Pb/Fe ratios. Sediment Pb concentrations were highest in 1990 and 2021, with lower values recorded in the intervening years. However, due to the limited sample sizes available for the intermediate years (n = 14 for each of 2001, 2003, 2005, and 2007) and for 2021 (n = 9), these temporal comparisons should be interpreted with caution. Finally, simulations incorporating acidification and increased sea surface temperature (SST) over the study period showed a 5.9 % increase in the concentration of bioavailable Pb^{2+}, rising from 1.41 × 10^{-7} mol L^{-1} in 1990 to1.49 × 10^{-7} mol L^{-1} in 2021.

3.2. Isotopic ratios and temporal trends

The $^{206}Pb/^{207}Pb$ ratios ranged from 1.125 to 1.233 (median = 1.175), and $^{208}Pb/^{206}Pb$ from 2.021 to 2.136 (median = 2.088). Samples from northern rias generally exhibited lower $^{206}Pb/^{207}Pb$ ratios compared to those from southern sites, whereas $^{208}Pb/^{206}Pb$ were higher. No clear inner-to-outer rias pattern was observed, and accordingly, no significant differences between species were detected. Samples from rias known for their higher industrial and anthropogenic influence (e.g., rias d, e, f, q, and r) exhibited lower $^{206}Pb/^{207}Pb$ and higher $^{208}Pb/^{206}Pb$ ratios compared to others. No consistent inner–outer gradient or interspecific differences were observed (Figs. S3, S4).

Both ratios shifted significantly over time, with $^{206}Pb/^{207}Pb$ increasing and $^{208}Pb/^{206}Pb$ decreasing. These trends were consistent across site-level analyses (Wilcoxon and Friedman tests) and full-dataset comparisons (Kruskal–Wallis test), with $p << 0.001$ for all tests except Friedman for $^{208}Pb/^{206}Pb$ ($p = 3.7 \times 10^{-3}$; Fig. 3). The strongest changes occurred between 1990 and 2021 ($p << 0.001$), though 1990 also differed from 2001–2007 (except 2007 for $^{206}Pb/^{207}Pb$). Years 2001–2007 showed similar $^{208}Pb/^{206}Pb$ ratios, while $^{206}Pb/^{207}Pb$ in 2007 was significantly lower than in 2001–2005 ($p < 0.005$). In 2021, values differed from 2001–2007, with minor exceptions (2003 in Friedman tests, and 2001–2003 in Kruskal–Wallis for $^{208}Pb/^{206}Pb$). At the sampling site level, trends were consistent with an overall rise in $^{206}Pb/^{207}Pb$ and decline in $^{208}Pb/^{206}Pb$, without a clear spatial pattern (Figs. S5, S6). A similar pattern in isotopic ratios was observed among the 50 samples showing the highest Pb concentrations.

Isotopic ratios of reference materials are shown in Table 1. Rocks had

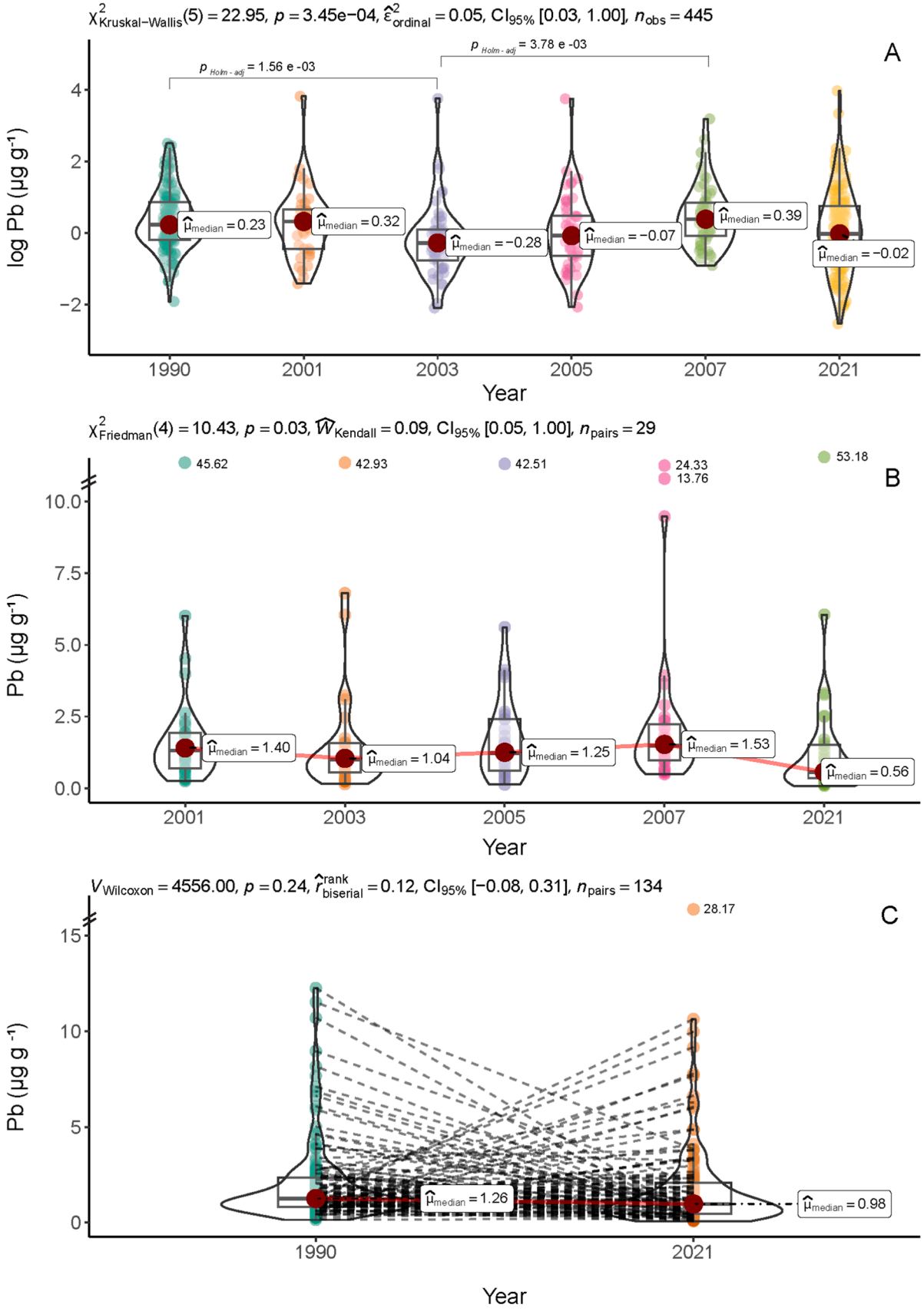

Fig. 2. Pb concentrations over time. Overview of Pb concentrations (µg g^{-1} dry weight) temporal trends: (A) Boxplots (logarithmic scale) with statistical summaries, with significance assessed using the Kruskal-Wallis test followed by Dunn's post-hoc analysis (B) repeated samples from 2001, 2003, 2005, 2007, and 2021 analyzed by Friedman test and Durbin Conover post-hoc analysis, and C) paired samples from 1990 and 2021 analyzed by Wilcoxon paired test. P-values showed only significant pairwise comparisons ($p < 0.05$).

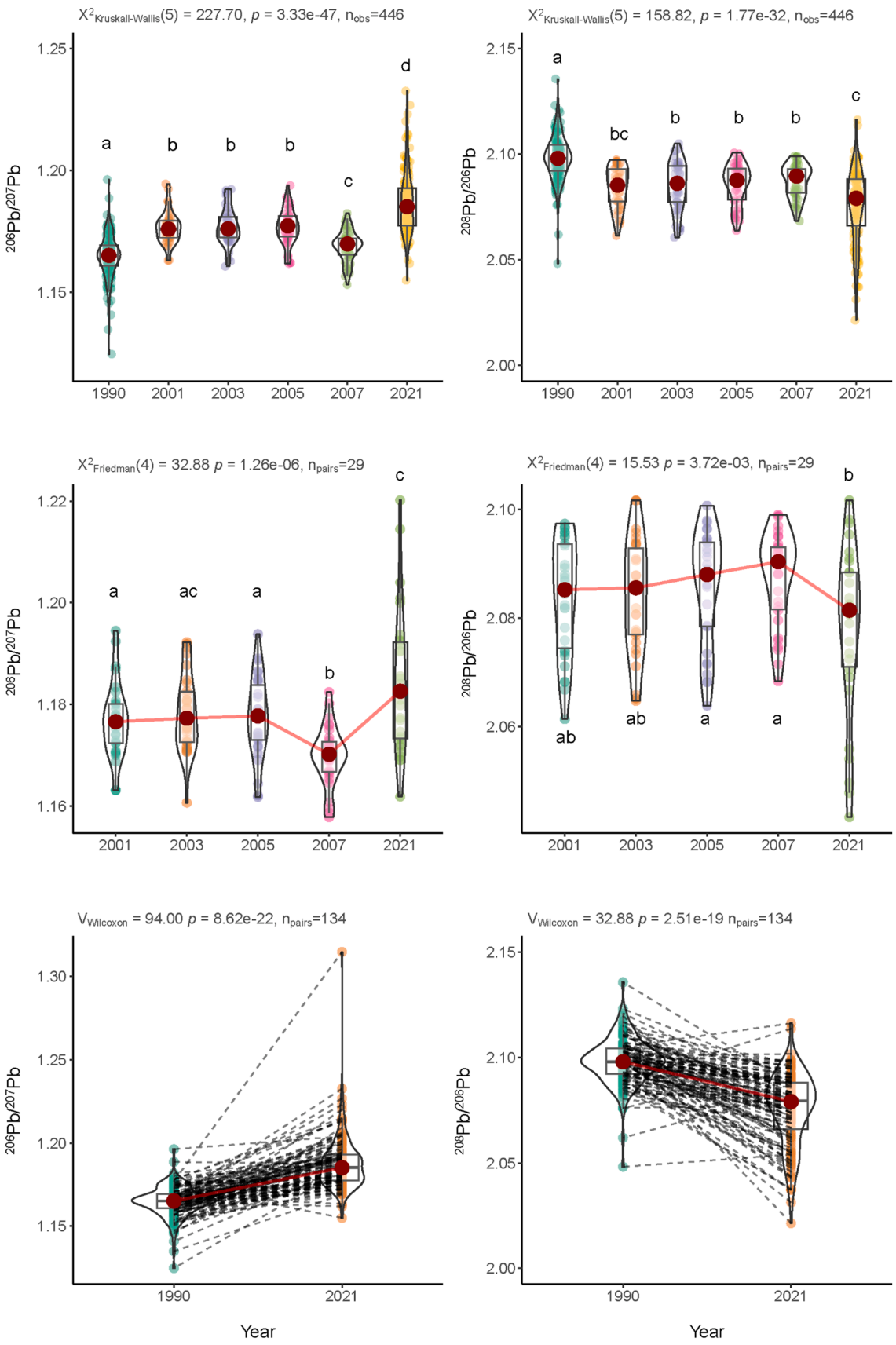

Fig. 3. $^{206}Pb/^{207}Pb$ and $^{208}Pb/^{206}Pb$ over time. Overview of $^{206}Pb/^{207}Pb$ and $^{208}Pb/^{206}Pb$ temporal trends: (A) Boxplots with statistical summaries, with significance assessed using the Kruskal-Wallis test followed by Dunn's post-hoc analysis; (B) Repeated measures from 2001, 2003, 2005, 2007 and 2021 analyzed by Friedman test and Durbin Conover post-hoc analysis; (C) Paired samples from 1990 and 2021 analyzed by Wilcoxon paired test. Distinct lowercase letters indicate significant differences between years (no shared letters = significant, $p < 0.05$).

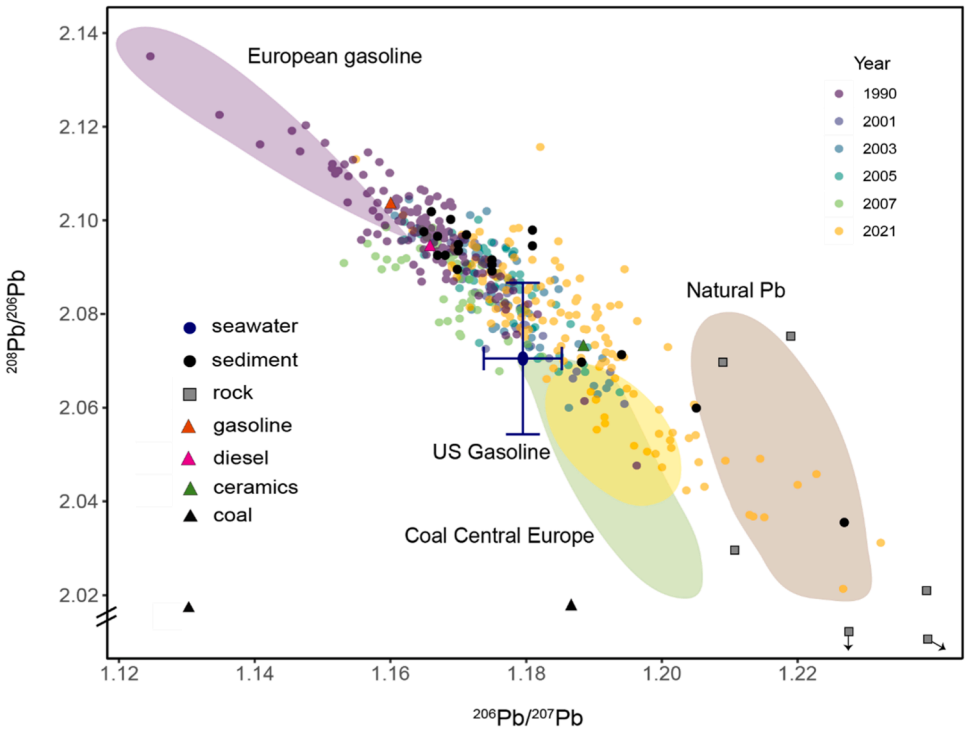

Fig. 4. Three-isotope plot of $^{206}Pb/^{207}Pb$ and $^{208}Pb/^{206}Pb$ ratios for samples of *Fucus vesiculosus* collected in 1990, 2001, 2003, 2005, 2007, and 2021. Samples are color-coded by the year of collection. Shaded areas represent isotopic contributions from different worldwide sources as reviewed by Komárek et al# (2008). Reference values for seawater [78–80] and coal from the study area [54] were obtained from the literature. Other reference materials from the study area are also plotted and listed in the legend.

higher $^{206}Pb/^{207}Pb$ (1.236 ± 0.036) and lower $^{208}Pb/^{206}Pb$ (2.009 ± 0.077) than sediments (1.177 ± 0.014 and 2.088 ± 0.015, respectively). Gasoline and diesel showed similar ratios between them. Ceramics plotted in an intermediate position, without a clearly distinctive isotopic signature. Sediment and algal samples from the same site were significantly correlated (rho = 0.49, $p = 0.03$ for $^{206}Pb/^{207}Pb$; rho = 0.64, $p = 0.003$ for $^{208}Pb/^{206}Pb$).

3.3. Pb sources

The three-isotope plot (Fig. 4) showed a strong correlation between $^{206}Pb/^{207}Pb$ and $^{208}Pb/^{206}Pb$ (rho = −0.84, $p < 2.2 \times 10^{-16}$), but no significant relationship was found between $^{206}Pb/^{207}Pb$ and the inverse of Pb concentrations (rho = 0.11, p = 0.078), indicating that isotopic variation is independent of total Pb levels. When grouping samples by whether Pb concentrations increased or decreased between 1990 and 2021, we observed that shifts in $^{206}Pb/^{207}Pb$ were slightly greater in samples where Pb levels declined; however, this difference was not statistically significant (Wilcoxon test, $p = 0.079$, Fig. S7). Spatial and temporal patterns further support these trends: samples from 1990 clustered near European leaded petrol signatures, while those from 2001 to 2007 occupied intermediate positions reflecting mixed contributions from unleaded petrol, diesel, ceramics, and other anthropogenic Pb sources reported in the literature (Table 1). By 2021, samples aligned more closely with natural sources, such as Galician rock formations (Fig. 4).

MixSIAR results confirmed this temporal shift: in 1990, Pb inputs were dominated by petrol (46.9 %) and coal (48.4 %), with 4.7 % from geological sources. By 2001–2007, petrol (38.9 %) and coal (40.1 %) decreased. In 2021, natural sources dominated (61.5 %), with reduced petrol (32.2 %) and coal (6.3 %) inputs, pointing to a long-term decline in anthropogenic Pb sources (Fig. S8).

4. Discussion

4.1. Trends in Pb concentrations

Lead pollution has driven one of the most transformative environmental regulations in history: the global phase-out of leaded gasoline [83]. This regulatory measure, along with reductions in industrial emissions and improved waste management [84], has significantly lowered environmental Pb inputs in recent decades [85]. Consequently, widespread declines in Pb levels have been reported in seawater [79], sediments [86], and marine biota [31]. Global meta-analyses on *Fucus* spp. indicate sustained reductions since the 1970s, though the rate of decrease has slowed since the early 2000s [87].

In contrast, our study shows only modest decreases in Pb concentrations in *Fucus* spp. from the Northeast Atlantic Ocean over the past 30 years. Specifically, we observed a 21.9 % median reduction across sampling stations (Fig. S2), with slight, non-significant downward trends from 1990 to 2021 (Fig. 2). This is consistent with previous regional studies reporting no significant changes between 2015 and 2019 in *F. vesiculous* [88], and even an increased Pb pollution probability in mosses from 2014 relative to 2000 [89]. In addition, these limited changes contrast with the pronounced declines observed for other Potentially Toxic Elements (e.g., Hg, Cd, Cr) in the same sites and period [90].

Despite the limited temporal decline, the median Pb concentration in our dataset (1.02 μg g^{-1} dry weight) is notably lower than the world median for *Fucus* spp. (2.87 μg g^{-1}) [87], suggesting limited Pb pollution impact for these populations. Most samples fall below the EU safety limit for edible seaweeds (3.0 μg g^{-1}) [91], though 60 samples exceeded this threshold, identifying areas of concern. The highest Pb concentrations were consistently recorded in the Ria do Burgo and Ria de Vigo (rias d and r, respectively, in Fig. S1), both of which have a history of intense industrial activity [92,93]. In these highly impacted sites, Pb concentrations remain elevated and stable over time.

Species-specific differences were observed: *F. ceranoides*, found in inner estuarine areas, exhibited higher Pb concentrations than *F. vesiculosus–F. spiralis,* which dominate more open, marine-influenced zones [94,95]. However, temporal trends were similar across species, suggesting that environmental factors rather than intrinsic physiological differences primarily drive the observed patterns, which is consistent with studies showing no significant interspecific differences under similar environmental conditions [81,82].

4.2. Changes in Pb isotopic composition and source apportionment

Over the 30-year study period, isotopic ratios ($^{206}Pb/^{207}Pb$ and $^{208}Pb/^{206}Pb$) showed clear temporal shifts from signatures characteristic of anthropogenic sources, such as regional ores, European leaded and unleaded gasoline, ceramics, waste incineration, and industrial aerosols, towards more natural (geogenic) values (Fig. 4, Table 1) [18,93]. These trends are consistent with previous sediment-based isotopic studies in the region [93].

MixSIAR source apportionment models reinforce this transition, showing a marked decline in anthropogenic contributions over time. Coal-related Pb inputs decreased sharply from 48.4 % in 1990 to 6.3 % in 2021, in line with the 2020 shutdown or downsizing of the region's main coal power plants (As Pontes, 1468.5 MW; and Cerceda-Meirama, 580 MW) [96]. Similarly, petrol-related inputs declined from 46.9 % to 32.2 %, indicating that traffic remains a diffuse, albeit diminished, source of Pb pollution [9]. Conversely, natural contributions increased from 4.7 % to 61.5 %.

These results suggest the effectiveness of environmental regulations over recent decades, including the ban on leaded fuel [6], and the implementation of the Urban Waste Water Treatment Directive [97], the Water Framework Directive [98], and the Marine Strategy Framework Directive [99]. These measures have contributed to improved wastewater treatment and reduced industrial emissions to coastal waters [84,90]. While major changes in isotopic signatures were expected around the 1990s–2000s due to the leaded petrol phase-out, continued shifts over time suggest that multiple regulatory interventions have played a role.

Median isotopic ratios fall within the range reported for North Atlantic seawater, mussels, and other seaweeds (Table 1, Fig. S9) while still showing sufficient variability to differentiate Pb sources. No significant isotopic differences were detected between *Fucus* species or between inner and outer ria zones, indicating no species-specific fractionation and suggesting spatially homogeneous Pb sources across habitats.

Spatial isotopic patterns further reflect anthropogenic influence: rias with long-standing industrial activity and urban population, such as Pontevedra (paper industry), Vigo (ceramics, automotive), Ferrol (metallurgy, shipyards), and O Burgo (fertilizers, chemicals) [34], exhibited lower $^{206}Pb/^{207}Pb$ ratios and higher $^{208}Pb/^{206}Pb$ ratios (Fig. S3, S4).

Interestingly, except for some heavily industrialized and populated rias, southern rias tended to exhibit higher $^{206}Pb/^{207}Pb$ and lower $^{208}Pb/^{206}Pb$ ratios than northern ones. This may be partly explained by regional geology: the southern rias are predominantly composed of alkaline and calc-alkaline granites, which have naturally higher $^{206}Pb/^{207}Pb$ and lower $^{208}Pb/^{206}Pb$ signatures compared to the slates and peridotites common in the north (Table 1) [33].

Finally, isotopic ratios in algae moderately correlated with those in sediments (rho = 0.49, $p = 0.03$ for $^{206}Pb/^{207}Pb$; rho = 0.64, $p = 0.003$ for $^{208}Pb/^{206}Pb$), likely reflecting differences in integration timescales. While algae reflect Pb exposure over days to weeks [100], the 5-mm sediment layers analyzed here reflect contamination over months to years [101,102]. This highlights the value of algal isotopic signatures for detecting recent shifts in Pb sources with greater temporal resolution than sediment analyses.

4.3. Factors explaining observed trends

As previously discussed, Pb concentrations in *Fucus* spp. did not show a significant decline over time, despite a clear shift in isotopic ratios ($^{206}Pb/^{207}Pb$ and $^{208}Pb/^{206}Pb$) toward more natural signatures. This decoupling suggests complex environmental dynamics. Notably, although not statistically significant ($p = 0.079$, Fig. S7), changes in $^{206}Pb/^{207}Pb$ between 1990 and 2021 tended to be slightly larger in those sites where Pb concentrations declined, suggesting that reductions in Pb load may be accompanied by more pronounced source shifts.

On one hand, this pattern may reflect the persistence of Pb inputs despite regulatory advances. Emerging sources, like batteries, electronic waste, or other modern materials, have intensified in recent years [103,104], and long-range atmospheric transport from other regions may also contribute [105]. However, these sources do not typically exhibit natural-like isotopic signatures, weakening this hypothesis. Similarly, the remobilization of legacy Pb from sediments [106] is an unlikely explanation, as such Pb usually retains anthropogenic isotopic fingerprints, contrary to the observed natural trend.

Alternatively, environmental Pb levels may indeed have declined, but this reduction may not be reflected in algae due to increased sediment contribution in 2021 (189 % compared to 13–49 % between 1990–2007). As sediments often carry high Pb loads, their accumulation on algal surfaces may elevate measured concentrations, masking a true decline in dissolved Pb. Previous studies report substantial sediment contributions to algal Pb ranging from 28–112 % [107–109]. Thus, although the same sampling washing protocol [110] was followed in 2021, persistent sediment particles were visually detected after rinsing. This, combined with strong Fe–Pb correlations and the observed decline in Pb/Fe ratios in algae in 2021 –indicating a real decrease in Pb when normalized to sediment-associated Fe– support this interpretation. Variability in sediment adhesion may arise from environmental factors such as enhanced terrestrial runoff due to storms or heavy rainfall, reduced water movement that limits natural cleaning of the thallus, or shifts in salinity and circulation patterns affecting particle deposition. Sediment contamination remains a well-known limitation in biomonitoring, and no method has proven fully effective at removing all particles without compromising tissue integrity.

In parallel, increased Pb bioavailability under changing environmental conditions may help explain stable concentrations despite lower inputs. This interpretation is supported by speciation simulations using Visual MINTEQ, which indicate a 5.9 % increase in free Pb^{2+} concentrations between 1990 and 2021. These results align with other studies [111,112].

Additionally, factors like intense rainfall [113] and rising temperature [114] may also promote Pb uptake. Despite differing concentrations especially elevated in *F. ceranoides*, no isotopic differences were observed among species, suggesting that the difference in metal uptake is driven by bioavailability, not source heterogeneity. Similarly, the most polluted sites exhibited stable concentrations but isotopic shifts toward natural values, indicating changes in source contribution rather than total load. Weak correlations between algal and seawater Pb concentrations [115] further support the idea that algae primarily reflect the bioavailable Pb fraction. However, the lack of high-resolution, long-term physicochemical data limits a proper evaluation of environmental drivers on Pb bioavailability.

Biological processes may also play a role. Elevated pCO_2 can induce oxidative stress and alter metal binding mechanisms [116,117]. Since Pb is mainly bound to cell walls (Vázquez-Arias et al., submitted), increased cell wall polysaccharide production under stress [118] could enhance Pb retention. Genetic or epigenetic adaptations may further influence Pb accumulation [119].

In addition, natural biological variability could itself explain the absence of clear temporal trends in some cases, especially when concentrations fall within the range of background fluctuation. However, in sites with historically high Pb pollution, algae consistently reflected the

contaminated status over time. For instance, samples from the inner parts of the Ría de Vigo and the Ría do Burgo remained highly enriched in Pb and showed isotopic signatures characteristic of intense anthropogenic sources. This suggests that while subtle changes may be obscured by biological noise, algae remain effective qualitative indicators of severe contamination.

Taken together, the results suggest that increased sediment contribution and enhanced bioavailability, both shaped by evolving environmental conditions, are key drivers of the observed stability in algal Pb concentrations, despite declining anthropogenic inputs. This interpretation is supported by isotopic data and MixSIAR modelling (Fig. S8), which consistently indicate a growing dominance of natural Pb sources in recent years, and consistent with emission trends [120] and regulatory milestones [90]. Yet the sustained Pb levels in biota remain a cause for concern, potentially offsetting the benefits achieved through emission reductions.

4.4. Limitations and future research

This study has several limitations that should be considered when interpreting the results. A key constraint is the limited availability of Pb isotopic data for the region. While MixSIAR provides useful insights, the lack of isotopic signatures for regional industrial sources and the uncertainty regarding the origin and composition of historically used coal hinder a complete reconstruction of source contributions. By generating new baselines across sites, materials, and years, this study begins to fill those gaps.

Another major limitation is the variable influence of sediment over time. The high estimated sediment contribution, especially in 2021, suggests that sediment-bound Pb can significantly elevate total tissue concentrations, potentially masking trends in dissolved or bioavailable Pb. This effect is difficult to correct for, as no washing protocol can remove attached sediment particles entirely without damaging the algal tissue, further complicating the interpretation of temporal patterns. Additionally, changes in environmental conditions, such as ocean acidification, ionic competition, and increased organic matter, may enhance Pb bioavailability, but the absence of long-term, high-resolution physicochemical data in the study area limits our capacity to assess these effects.

Biological variability and the complexities of field sampling introduce uncertainty but also represent a key strength: biomonitors provide organism-level insight that sediment or water analyses alone cannot capture. Given the often weak correlations among environmental compartments, separate assessments remain essential. Expanding this approach to other ecologically important species and increasing the temporal resolution through more frequent sampling would improve the detection of subtle trends in Pb concentrations and source dynamics.

Finally, the use of quadrupole ICP-MS, rather than more precise methods like MC-ICP-MS with resin purification, may introduce analytical bias. To assess the potential impact of matrix effects, six samples were subjected to anion-exchange purification and compared with their untreated counterparts, yielding negligible differences. We acknowledge that this limited comparison may not fully capture all potential inaccuracies, particularly in samples with low Pb concentrations, and that such uncertainties could influence the input data used in the MixSIAR model. Nevertheless, our rigorous quality control procedures, including the use of certified reference materials and analytical replicated, helped minimize this risk.

In light of these limitations, future research should focus on expanding regional isotopic datasets for key sources, incorporating long-term physicochemical monitoring to better understand the drivers of Pb bioavailability, and applying isotopic tools to a broader range of ecologically relevant species. These efforts will enhance the resolution and interpretation of metal pollution trends in coastal ecosystems and strengthen the role of biomonitors in environmental assessment.

5. Conclusions

This study provides one of the most comprehensive long-term datasets to date on Pb concentrations and isotopic signatures in marine organisms, specifically *Fucus* spp., from a coastal region where such information is extremely scarce.

Despite decades of regulatory action, including the global phase-out of leaded gasoline, our results reveal only modest declines in Pb concentrations in *Fucus* spp. from the Northeast Atlantic over the past 30 years. In contrast, Pb isotopic signatures show a clear and consistent shift from anthropogenic to more natural sources between 1990 and 2021, as confirmed by MixSIAR modelling.

These findings highlight the limitations of relying solely on concentration data and underscore the value of Pb isotopes in disentangling changes in pollution sources. However, in highly contaminated areas, *Fucus* spp. continues to serve as a reliable biomonitor, reflecting elevated Pb concentrations. By using marine organisms, the study goes beyond measuring environmental levels, capturing instead the fraction of Pb that is biologically available and potentially bioaccumulative.

The results also emphasize the importance of long-term monitoring: shifts in source contributions and environmental processes are only evident over multi-decadal timescales. By integrating isotopic and biological data across 30 years, this study captures subtle but meaningful trends that would remain undetected in short-term assessments.

Overall, our results point to a long-term reduction in anthropogenic Pb inputs but also expose the complex biogeochemical behavior of Pb in marine environments, shaped by sediment interaction, redox dynamics, and ocean chemistry. The new isotopic baseline data presented here fills a critical gap for the Northeast Atlantic and offers a valuable reference for future source apportionment and environmental assessments. Continued monitoring and sustained regulatory action remain necessary to further reduce Pb pollution and safeguard coastal ecosystems.

Environmental implication

While isotopic data support the effective reduction of anthropogenic Pb inputs to the Northeast Atlantic, stable concentrations in *Fucus* spp. suggest an increasing influence of sediment-derived Pb and bioavailability driven by acidification. This shift highlights critical gaps in concentration-based monitoring, demanding the integration of isotope fingerprinting into regulatory frameworks to identify Pb sources, especially in estuaries, where sediment disturbance and climate change may maintain elevated Pb uptake by organisms despite declines in anthropogenic Pb sources.

CRediT authorship contribution statement

Adéla Šípková: Writing – review & editing. **Michael Komárek:** Writing – review & editing, Conceptualization. **Vladislav Chrastný:** Writing – review & editing. **Pacin Carme:** Writing – review & editing, Writing – original draft, Formal analysis. **Jesús R. Aboal:** Writing – review & editing, Funding acquisition, Conceptualization. **J. Ángel Fernández:** Writing – review & editing, Funding acquisition, Conceptualization. **Antón Vázquez-Arias:** Writing – review & editing.

Declaration of Generative AI and AI-assisted technologies in the writing process

During the preparation of this work the authors used chat GPT in order to improve readability and language. After using this tool, the authors reviewed and edited the content as needed and take full responsibility for the content of the publication.

Declaration of Competing Interest

The authors declare that they have no known competing financial

interests or personal relationships that could have appeared to influence the work reported in this paper.

Acknowledgments

C. Pacín was supported by a predoctoral grant from Xunta de Galicia (ED481A 2022/374) and a research stay grant from CRETUS, which enabled isotope measurements during her stay in the Czech Republic. We sincerely thank Dr. Teresa Taboada for her assistance in selecting representative rock formations from the study area. We also thank Julia Bairstow for her careful revision of the English language. Finally, we thank the anonymous reviewers for their constructive comments, which significantly improved the quality of the manuscript.

Appendix A. Supporting information

Supplementary data associated with this article can be found in the online version at doi:10.1016/j.jhazmat.2025.139289.

Data availability

Data will be made available on request.

References

[1] Singh, N., Kumar, A., Gupta, V.K., Sharma, B., 2018. Biochemical and molecular bases of lead-induced toxicity in mammalian systems and possible mitigations. Chem Res Toxicol 31 (10), 1009–1021. https://doi.org/10.1021/ACS.CHEMRESTOX.8B00193/ASSET/IMAGES/MEDIUM/TX-2018-00193E_0007.GIF.

[2] Rahman, Z., Singh, V.P., 2019. The relative impact of toxic heavy metals (THMs) (Arsenic (As), Cadmium (Cd), Chromium (Cr)(VI), Mercury (Hg), and Lead (Pb)) on the total environment: an overview. Environ Monit Assess 191 (7), 1–21. https://doi.org/10.1007/S10661-019-7528-7/TABLES/3.

[3] Garrett, R.G., 2000. Natural sources of metals to the environment. Hum Ecol Risk Assess 6 (6), 945–963. https://doi.org/10.1080/10807030091124383.

[4] Obeng-Gyasi, E., 2019. Sources of lead exposure in various countries. Rev Environ Health 34 (1), 25–34. https://doi.org/10.1515/REVEH-2018-0037/MACHINEREADABLECITATION/RIS.

[5] Raj, K., Das, A.P., 2023. Lead pollution: impact on environment and human health and approach for a sustainable solution. Environ Chem Ecotoxicol 5, 79–85. https://doi.org/10.1016/J.ENCECO.2023.02.001.

[6] Ritchie, Hanna, 2022. How the World eliminated lead from gasoline. Our World data. ⟨https://ourworldindata.org/leaded-gasoline-phase-out⟩ (accessed 2024-11-29).

[7] Chavez-Garcia, J.A., Noriega-León, A., Alcocer-Zuñiga, J.A., Robles, J., Cruz-Jiménez, G., Juárez-Pérez, C.A., Martinez-Alfaro, M., 2022. Association between lead source exposure and blood lead levels in some lead manufacturing countries: a systematic review and meta-analysis. J Trace Elem Med Biol 71, 126948. https://doi.org/10.1016/J.JTEMB.2022.126948.

[8] Arfala, Y., Douch, J., Assabbane, A., Kaaouachi, K., Tian, H., Hamdani, M., 2018. Assessment of heavy metals released into the air from the cement kilns Co-burning waste: case of Oujda cement manufacturing (Northeast Morocco). Sustain Environ Res 28 (6), 363–373. https://doi.org/10.1016/J.SERJ.2018.07.005.

[9] Chrastný, V., Šillerová, H., Vítková, M., Francová, A., Jehlička, J., Kocourková, J., Aspholm, P.E., Nilsson, L.O., Berglen, T.F., Jensen, H.K.B., Komárek, M., 2018. Unleaded gasoline as a significant source of Pb emissions in the subarctic. Chemosphere 193, 230–236. https://doi.org/10.1016/j.chemosphere.2017.11.031.

[10] Zhou, Q., Wang, S., Liu, J., Hu, X., Liu, Y., He, Y., He, X., Wu, X., 2022. Geological evolution of offshore pollution and its long-term potential impacts on marine ecosystems. Geosci Front 13 (5), 101427. https://doi.org/10.1016/J.GSF.2022.101427.

[11] Sharifi, Z., Hossaini, S.M.T., Renella, G., 2016. Risk assessment for sediment and stream water polluted by heavy metals released by a municipal solid waste composting plant. J Geochem Explor 169, 202–210. https://doi.org/10.1016/j.gexplo.2016.08.001.

[12] Boyle, E.A., Lee, J.M., Echegoyen, Y., Noble, A., Moos, S., Carrasco, G., Zhao, N., Kayser, R., Zhang, J., Gamo, T., Obata, H., Norisuye, K., 2014. Anthropogenic lead emissions in the ocean: the evolving global experiment. Oceanography 27 (1), 69–75. https://doi.org/10.5670/OCEANOG.2014.10.

[13] Buck-Wiese, H., Andskog, M.A., Nguyen, N.P., Bligh, M., Asmala, E., Vidal-Melgosa, S., Liebeke, M., Gustafsson, C., Hehemann, J.H., 2023. Fucoid brown algae inject fucoidan carbon into the ocean. Proc Natl Acad Sci USA 120 (1), e2210561119. https://doi.org/10.1073/PNAS.2210561119/SUPPL_FILE/PNAS.2210561119.SAPP.PDF.

[14] Thomsen, M., South, P., Staehr, P., 2024. Fabulous but forgotten fucoid forests. Ecol Evol 14, e70491. https://doi.org/10.1002/ece3.70491.

[15] Pawlik-Skowrońska, B., Pirszel, J., Brown, M.T., 2007. Concentrations of phytochelatins and glutathione found in natural assemblages of seaweeds depend on species and metal concentrations of the habitat. Aquat Toxicol 83 (3), 190–199. https://doi.org/10.1016/J.AQUATOX.2007.04.003.

[16] Ramesh, K., Berry, S., Brown, M.T., 2015. Accumulation of silver by fucus Spp. (Phaeophyceae) and its toxicity to fucus ceranoides under different salinity regimes. Ecotoxicology 24 (6), 1250–1258. https://doi.org/10.1007/S10646-015-1495-8/TABLES/2.

[17] Sundhar, S., Arisekar, U., Shakila, R.J., Shalini, R., Al-Ansari, M.M., Al-Dahmash, N.D., Mythili, R., Kim, W., Sivaraman, B., Jenishma, J.S., Karthy, A., 2024. Potentially toxic metals in seawater, sediment and seaweeds: bioaccumulation, ecological and human health risk assessment. Environ Geochem Health 46 (2), 1–21. https://doi.org/10.1007/S10653-023-01789-0/TABLES/1.

[18] Komárek, M., Ettler, V., Chrastný, V., Mihaljevič, M., 2008. Lead isotopes in environmental sciences: a review. Environ Int 34 (4), 562–577. https://doi.org/10.1016/J.ENVINT.2007.10.005.

[19] Astray, B., Šípková, A., Baragaño, D., Pechar, J., Krejci, R., Komárek, M., Chrastný, V., 2024. Measuring Pb isotope ratios in fresh snow filtrate refines the apportioning of contaminant sources in the arctic. Environ Pollut 345, 123457. https://doi.org/10.1016/J.ENVPOL.2024.123457.

[20] Bohdalkova, L., Novak, M., Stepanova, M., Fottova, D., Chrastny, V., Mikova, J., Kubena, A.A., 2014. The fate of atmospherically derived Pb in central european catchments: insights from spatial and temporal pollution gradients and Pb isotope ratios. Environ Sci Technol 48 (8), 4336–4343. https://doi.org/10.1021/ES500393Z/SUPPL_FILE/ES500393Z_SI_007.PDF.

[21] Peng, B., Juhasz, A., Fang, X., Jiang, C., Wu, S., Li, X., Xie, S., Dai, Y., 2022. Lead isotopic fingerprinting as a tracer to identify the sources of heavy metals in sediments from the four rivers' inlets to Dongting Lake, China. Catena (Amst) 219, 106594. https://doi.org/10.1016/J.CATENA.2022.106594.

[22] Distribution of Pb Isotopes in Different Chemical Fractions in Bed Sediments from Lower Reaches of the Xiangjiang River, Hunan Province of China. *Science of The Total Environment* 2022, *829*, 154394. https://doi.org/10.1016/J.SCITOTENV.2022.154394.

[23] Le Croizier, G., Point, D., Renedo, M., Munaron, J.-M., Espinoza, P., Amezcua-Martinez, F., Lanco Bertrand, S., Lorrain, A., 2022. Mercury concentrations, biomagnification and isotopic discrimination factors in two seabird species from the humboldt current ecosystem. Mar Pollut Bull 177, 113481. https://doi.org/10.1016/j.marpolbul.2022.113481.

[24] Søndergaard, J., Mosbech, A., 2022. Mining pollution in greenland - the lesson learned: a review of 50 years of environmental studies and monitoring. Sci Total Environ 812, 152373. https://doi.org/10.1016/j.scitotenv.2021.152373.

[25] Runcie, J.W., Townsend, A.T., Seen, A.J., 2009. The application of lead isotope ratios in the antarctic macroalga iridaea cordata as a contaminant monitoring tool. Mar Pollut Bull 58 (7), 961–966. https://doi.org/10.1016/j.marpolbul.2009.03.010.

[26] Soto-Jiménez, M.F., Páez-Osuna, F., Scelfo, G., Hibdon, S., Franks, R., Aggarawl, J., Flegal, A.R., 2008. Lead pollution in subtropical ecosystems on the SE Gulf of California coast: a study of concentrations and isotopic composition. Mar Environ Res 66 (4), 451–458. https://doi.org/10.1016/J.MARENVRES.2008.07.009.

[27] Søndergaard, J., Asmund, G., Johansen, P., Elberling, B., 2010. Pb isotopes as tracers of mining-related pb in lichens, seaweed and mussels near a former Pb-Zn mine in West Greenland. Environ Pollut 158 (5), 1319–1326. https://doi.org/10.1016/j.envpol.2010.01.006.

[28] Outridge, P.M., Evans, R.D., Wagemann, R., Stewart, R.E.A., 1997. Historical trends of heavy metals and stable lead isotopes in beluga (Delphinapterus leucas) and Walrus (Odobenus rosmarus Rosmarus) in the Canadian Arctic. Sci Total Environ 203 (3), 209–219. https://doi.org/10.1016/S0048-9697(97)00142-3.

[29] Kelly, A.E., Reuer, M.K., Goodkin, N.F., Boyle, E.A., 2009. Lead concentrations and isotopes in corals and water near Bermuda, 1780–2000. Earth Planet Sci Lett 283 (1–4), 93–100. https://doi.org/10.1016/J.EPSL.2009.03.045.

[30] Couture, R.M., Chiffoleau, J.F., Auger, D., Claisse, D., Gobeil, C., Cossa, D., 2010. Seasonal and decadal variations in lead sources to eastern North Atlantic mussels. Environ Sci Technol 44 (4), 1211–1216. https://doi.org/10.1021/ES902352Z/SUPPL_FILE/ES902352Z_SI_001.PDF.

[31] Barreira, J., Araújo, D.F., Knoery, J., Briant, N., Machado, W., Grouhel-Pellouin, A., 2024. The french mussel watch program reveals the attenuation of coastal lead contamination over four decades. Mar Pollut Bull 199, 115975. https://doi.org/10.1016/J.MARPOLBUL.2023.115975.

[32] Mapas Climáticos de España y ETo - Agencia Estatal de Meteorología - AEMET. Gobierno de España.

[33] Xunta de Galicia. *Atlas Geoquímico de Galicia*; 1992.

[34] PRTR España. *Registro Estatal de Emisiones y Fuentes Contaminantes*.

[35] García-Seoane, R., Fernández, J.A., Villares, R., Aboal, J.R., 2018. Use of macroalgae to biomonitor pollutants in coastal waters: optimization of the methodology. Ecol Indic 84, 710–726. https://doi.org/10.1016/j.ecolind.2017.09.015.

[36] Wallace, A.L., Klein, A.S., Mathieson, A.C., 2004. Determining the affinities of salt marsh fucoids using microsatellite markers: evidence of hybridization and introgression between two species of fucus (Phaeophyta) in a maine estuary. J Phycol 40 (6), 1013–1027. https://doi.org/10.1111/j.1529-8817.2004.04085.x.

[37] Almeida, S.C., Neiva, J., Sousa, F., Martins, N., Cox, C.J., Melo-Ferreira, J., Guiry, M.D., Serrão, E.A., Pearson, G.A., 2022. A low-latitude species pump: peripheral isolation, parapatric speciation and mating-system evolution converge

in a marine radiation. Mol Ecol 31 (18), 4797–4817. https://doi.org/10.1111/MEC.16623.
[38] Viana, I.G., Aboal, J.R., Fernández, J.A., Real, C., Villares, R., Carballeira, A., 2010. Use of macroalgae stored in an environmental specimen bank for application of some european framework directives. Water Res 44 (6), 1713–1724. https://doi.org/10.1016/J.WATRES.2009.11.036.
[39] National Institute of Standards and Technology. *Standard Reference Material 3328 Lead (Pb) Isotopic Standard Solution CERTIFICATE OF ANALYSIS*; 2023.
[40] Judd, C.D., Swami, K., 2010. ICP-MS determination of lead isotope ratios in legal and counterfeit cigarette tobacco samples. Isot Environ Health Stud 46 (4), 484–494. https://doi.org/10.1080/10256016.2010.528839.
[41] Ďurišová, J., Ackerman, L., Strnad, L., Chrastný, V., Borovička, J., 2015. Lead isotopic composition in biogenic certified reference materials determined by different ICP-based mass spectrometric techniques. Geostand Geoanal Res 39 (2), 209–220. https://doi.org/10.1111/J.1751-908X.2014.00280.X.
[42] *GeoReM: Geological and Enviornmental Reference Materials*. Max Planck Gesellschaft. https://doi.org/10.1111/GGR.12460.
[43] R Core Team. R: A Language and Environment for Statistical Computing, Version 4.4.1. R Foundation for Statistical. 2024.
[44] Fox J.; Weisberg S. *An R Companion to Applied Regression.*, Third.; Sage: Thousand Oaks CA., 2019; Vol. Third edition.
[45] Wickham, H., 2016. Ggplot2: Elegant Graphics for Data Analysis. Springer-Verlag, New York.
[46] Patil, I., 2021. Visualizations with statistical details: the "ggstatsplot" approach. J Open Source Softw 6 (61), 3167. https://doi.org/10.21105/joss.03167.
[47] Stock, B.C., Jackson, A.L., Ward, E.J., Parnell, A.C., Phillips, D.L., Semmens, B.X., 2018. Analyzing mixing systems using a new generation of Bayesian tracer mixing models. PeerJ 6, e5096. https://doi.org/10.7717/peerj.5096.
[48] QGIS Development Team, 2024. QGIS Geographic Information System, Version 3.36.3. 2024.
[49] Gustafsson, J.P. Visual MINTEQ Version 3.1. KTH Royal Institute of Technology, Department of Land and Water Resources Engineering, Stockholm, Sweden. 2013.
[50] Padin, X.A., Velo, A., Pérez, F.F., 2020. ARIOS: a database for ocean acidification assessment in the iberian upwelling system (1976-2018). Earth Syst Sci Data 12 (4), 2647–2663. https://doi.org/10.5194/ESSD-12-2647-2020.
[51] Zhang, X., Zhang, Y., Ding, D., Zhao, J., Liu, J., Yang, W., Qu, K., 2016. On-site determination of Pb2 + and Cd2 + in seawater by double stripping voltammetry with bismuth-modified working electrodes. Microchem J 126, 280–286. https://doi.org/10.1016/J.MICROC.2015.12.010.
[52] Zhang, X., Ma, S., Cui, Z., Chen, J., Cui, Y., Zhao, J., Feng, X., 2011. Sensitive determination of trace Pb2+ in seawater using columnar glassy carbon electrode. J Chin Chem Soc 58 (5), 681–687. https://doi.org/10.1002/JCCS.201190106.
[53] Sugden, C.L., Farmer, J.G., MacKenzie, A.B., 1993. Isotopic ratios of lead in contemporary environmental material from Scotland. Environ Geochem Health 15 (2), 59–65. https://doi.org/10.1007/BF02627823.
[54] Díaz-Somoano, M., Suárez-Ruiz, I., Alonso, J.I.G., Ruiz Encinar, J., López-Antón, M.A., Martínez-Tarazona, M.R., 2007. Lead isotope ratios in Spanish coals of different characteristics and origin. Int J Coal Geol 71 (1), 28–36. https://doi.org/10.1016/j.coal.2006.05.006.
[55] Díaz-Somoano, M., Kylander, M.E., López-Antón, M.A., Suárez - Ruiz, I., Martínez-Tarazona, M.R., Ferrat, M., Kober, B., Weiss, D.J., 2009. Stable lead isotope compositions in selected coals from around the world and implications for present day aerosol source tracing. Environ Sci Technol 43 (4), 1078–1085. https://doi.org/10.1021/ES801818R/SUPPL_FILE/ES801818R_SI_001.PDF.
[56] Wang, Z., Dwyer, G.S., Coleman, D.S., Vengosh, A., 2019. Lead isotopes as a new tracer for detecting coal fly ash in the environment. Environ Sci Technol Lett 6 (12), 714–719. https://doi.org/10.1021/ACS.ESTLETT.9B00512/SUPPL_FILE/EZ9B00512_SI_001.PDF.
[57] Cloquet, C., Carignan, J., Libourel, G., 2006. Atmospheric pollutant dispersion around an urban area using trace metal concentrations and pb isotopic compositions in epiphytic lichens. Atmos Environ 40 (3), 574–587. https://doi.org/10.1016/J.ATMOSENV.2005.09.073.
[58] Plasencia Sánchez, E., Rosell, M., Torrentó, C., Sánchez-Soberón, F., Rovira, J., Sierra, J., Schuhmacher, M., Soler, A., Widory, D., 2025. Improving air pollution source apportionment in size-segregated PM using Pb isotope-based bayesian mixing models in tarragona (Spain). Atmos Res 316, 107939. https://doi.org/10.1016/J.ATMOSRES.2025.107939.
[59] Véron, A., Flament, P., Bertho, M.L., Alleman, L., Flegal, R., Hamelin, B., 1999. Isotopic evidence of pollutant lead sources in Northwestern France. Atmos Environ 33 (20), 3377–3388. https://doi.org/10.1016/S1352-2310(98)00376-8.
[60] Monna, F., Lancelot, J., Croudace, I.W., Cundy, A.B., Lewis, J.T., 1997. Pb isotopic composition of airborne particulate material from France and the Southern United Kingdom: implications for Pb pollution sources in urban areas. Environ Sci Technol 31, 2277–2286. https://doi.org/10.1021/ES960870.
[61] Chiaradia, M., Cupelin, F., 2000. Behaviour of airborne lead and temporal variations of its source effects in Geneva (Switzerland): comparison of anthropogenic versus natural processes. Atmos Environ 34 (6), 959–971. https://doi.org/10.1016/S1352-2310(99)00213-7.
[62] Novák, M., Emmanuel, S., Vile, M.A., Erel, Y., Véron, A., Pačes, T., Wieder, R.K., Vaněček, M., Štěpánová, M., Břízová, E., Hovorka, J., 2003. Origin of lead in Eight central European peat bogs determined from isotope ratios, strengths, and operation times of regional pollution sources. Environ Sci Technol 37 (3), 437–445. https://doi.org/10.1021/ES0200387;SUBPAGE:STRING:ABSTRACT;JOURNAL:JOURNAL:ESTHAG;REQUESTEDJOURNAL:JOURNAL:ESTHAG;WGROUP:STRING:ACHS.
[63] Kylander, M.E., Klaminder, J., Bindler, R., Weiss, D.J., 2010. Natural lead isotope variations in the atmosphere. Earth Planet Sci Lett 290 (1–2), 44–53. https://doi.org/10.1016/J.EPSL.2009.11.055.
[64] Tornos, F., Arias, D., 1993. Sulphur and lead isotope geochemistry of the rubiales Zn-Pb Ore deposit (NW Spain). Eur J Mineral 5 (4), 763–774. https://doi.org/10.1127/EJM/5/4/0763.
[65] Tornos, F., Ribera, F., Shepherd, T.J., Spiro, B., 1996. The geological and metallogenic setting of stratabound carbonate-hosted Zn-Pb mineralizations in the West Asturian Leonese Zone, NW Spain. Min Depos 31 (1–2), 27–40. https://doi.org/10.1007/BF00225393/METRICS.
[66] Arias Prieto, D. El Yacimiento de Pb-Zn de Rubiales (Lugo, España): Hipótesis Genética. 1989..
[67] Neiva, A.M.R., Andráš, P., Ramos, J.M.F., 2008. Antimony Quartz and antimony–gold Quartz veins from Northern Portugal. Ore Geol Rev 34 (4), 533–546. https://doi.org/10.1016/J.OREGEOREV.2008.03.004.
[68] Jorge Millos; Paula Álvarez; Beatriz Comendador. Provenance of the Prehistoric Silver Set of Antas de Ulla, North-Western Iberia, Using Lead Stable Isotope Ratios.
[69] Hansmann, W., Köppel, V., 2000. Lead-isotopes as tracers of pollutants in soils. Chem Geol 171 (1–2), 123–144. https://doi.org/10.1016/S0009-2541(00)00230-8.
[70] Carignan, J., Libourel, G., Cloquet, C., Le Forestier, L., 2005. Lead isotopic composition of fly ash and flue gas residues from municipal solid waste combustors in France: implications for atmospheric lead source tracing. Environ Sci Technol 39 (7), 2018–2024. https://doi.org/10.1021/ES048693X.
[71] Del Rio-Salas, R., Moreno-Rodríguez, V., Loredo-Portales, R., Salgado-Souto, S., Rader, S., Valencia-Moreno, M., Romo-Morales, D., Aguirre-Noyola, J.L., Ramos-Pérez, D., 2025. Do efflorescent salts from worn lead-acid automotive batteries represent potential non-exhaust emissions to urban pollution? A Pb isotope perspective. J Hazard Mater 488, 137366. https://doi.org/10.1016/J.JHAZMAT.2025.137366.
[72] Townsend, A.T., Snape, I., Palmer, A.S., Seen, A.J., 2009. Lead isotopic signatures in antarctic marine sediment cores: a comparison between 1 M HCl partial extraction and HF total digestion pre-treatments for discerning anthropogenic inputs. Sci Total Environ 408 (2), 382–389. https://doi.org/10.1016/J.SCITOTENV.2009.10.014.
[73] Jiang, S., Luo, J., Ye, Y., Yang, G., Pi, W., He, W., 2019. Using Pb isotope to quantify the effect of various sources on multi-metal polluted soil in Guiyu. Bull Environ Contam Toxicol 102 (3), 413–418. https://doi.org/10.1007/S00128-018-02534-5/FIGURES/3.
[74] Kylander, M.E., Weiss, D.J., Martínez Cortízas, A., Spiro, B., Garcia-Sanchez, R., Coles, B.J., 2005. Refining the pre-industrial atmospheric Pb isotope evolution curve in europe using an 8000 year old peat core from NW Spain. Earth Planet Sci Lett 240 (2), 467–485. https://doi.org/10.1016/J.EPSL.2005.09.024.
[75] Schleicher, N.J., Dong, S., Packman, H., Little, S.H., Ochoa Gonzalez, R., Najorka, J., Sun, Y., Weiss, D.J., 2020. A global assessment of copper, zinc, and lead isotopes in mineral dust sources and aerosols. Front Earth Sci 8, 492950. https://doi.org/10.3389/FEART.2020.00167/XML/NLM.
[76] Bollhöfer, A., Rosman, K.J.R., 2001. Isotopic source signatures for atmospheric lead: the Northern hemisphere. Geochim Cosmochim Acta 65 (11), 1727–1740. https://doi.org/10.1016/S0016-7037(00)00630-X.
[77] Zhang, X., Lemaitre, N., Rickli, J.D., Suhrhoff, T.J., Shelley, R., Benhra, A., Faye, S., Jeyid, M.A., Vance, D., 2024. Tracing anthropogenic aerosol trace metal sources in the North Atlantic ocean using Pb, Zn and Ni isotopes. Mar Chem 258, 104347. https://doi.org/10.1016/J.MARCHEM.2023.104347.
[78] Véron, A.J., church, T.M., Patterson, C.C., Flegal, A.R., 1994. Use of stable lead isotopes to characterize the sources of anthropogenic lead in North Atlantic surface waters. Geochim Cosmochim Acta 58 (15), 3199–3206. https://doi.org/10.1016/0016-7037(94)90047-7.
[79] Pinedo-González, P., West, A.J., Tovar-Sanchez, A., Duarte, C.M., Sañudo-Wilhelmy, S.A., 2018. Concentration and isotopic composition of dissolved Pb in surface waters of the modern global ocean. Geochim Cosmochim Acta 235, 41–54. https://doi.org/10.1016/J.GCA.2018.05.005.
[80] Zurbrick, C.M., Boyle, E.A., Kayser, R.J., Reuer, M.K., Wu, J., Planquette, H., Shelley, R., Boutorh, J., Cheize, M., Contreira, L., Barraqueta, J.L.M., Lacan, F., Sarthou, G., 2018. Dissolved Pb and Pb isotopes in the North Atlantic from the GEOVIDE Transect (GEOTRACES GA-01) and their decadal evolution. Biogeosciences 15 (16), 4995–5014. https://doi.org/10.5194/BG-15-4995-2018.
[81] Barreiro, R., Picado, L., Real, C., 2002. Biomonitoring heavy metals in estuaries: a field comparison of two brown algae species inhabiting upper estuarine reaches. Environ Monit Assess 2002 752 75 (2), 121–134. https://doi.org/10.1023/A:1014479612811.
[82] Carballeira, A., Carral, E., Puente, X., Villares, R., 2000. Regional-scale monitoring of coastal contamination. Nutrients and heavy metals in estuarine sediments and organisms on the coast of galicia (Northwest Spain). Int J Environ Pollut 13 (1/2/3/4/5/6), 534. https://doi.org/10.1504/IJEP.2000.002333.
[83] Von Storch, H., Costa-Cabral, M., Hagner, C., Feser, F., Pacyna, J., Pacyna, E., Kolb, S., 2003. Four decades of gasoline lead emissions and control policies in Europe: a retrospective assessment. Sci Total Environ 311 (1), 151–176. https://doi.org/10.1016/S0048-9697(03)00051-2.
[84] *Censo Nacional de Vertidos (CNV)*. ⟨https://www.miteco.gob.es/es/cartografia-y-sig/ide/descargas/agua/censo-nacional-vertidos.html⟩.
[85] *Heavy metal emissions in Europe (Indicator) | European zero pollution dashboards*. ⟨https://www.eea.europa.eu/en/european-zero-pollution-dashboards/indicators/heavy-metal-emissions-in-europe-indicator⟩ (accessed 2025-05-21).

[86] Logemann, A., Reininghaus, M., Schmidt, M., Ebeling, A., Zimmermann, T., Wolschke, H., Friedrich, J., Brockmeyer, B., Pröfrock, D., Witt, G., 2022. Assessing the chemical anthropocene – development of the legacy pollution fingerprint in the North Sea during the last century. Environ Pollut 302, 119040. https://doi.org/10.1016/J.ENVPOL.2022.119040.
[87] Aboal, J.R., Pacín, C., García-Seoane, R., Varela, Z., González, A.G., Fernández, J. A., 2023. Global decrease in heavy metal concentrations in brown algae in the last 90 years. J Hazard Mater 445, 130511. https://doi.org/10.1016/J.JHAZMAT.2022.130511.
[88] García-Seoane, R., Fernández, J.A., Boquete, M.T., Aboal, J.R., 2021. Analysis of intra-Thallus and temporal variability of trace elements and nitrogen in fucus vesiculosus: sampling protocol optimization for biomonitoring. J Hazard Mater 412, 125268. https://doi.org/10.1016/J.JHAZMAT.2021.125268.
[89] Giráldez, P., Crujeiras, R.M., Fernández, J.Á., Aboal, J.R., 2022. Establishment of background pollution levels and spatial analysis of moss data on a regional scale. Sci Total Environ 839, 156182. https://doi.org/10.1016/J.SCITOTENV.2022.156182.
[90] Pacín, C., Fernández, J.Á., Conde-Amboage, M., Lazzari, M., García-Seoane, R., G. Viana, I., Varela, Z., Real, C., Villares, R., Aboal, J.R., 2025. Three decades of change in potentially toxic elements in brown algae in the Northeast Atlantic Ocean. Environ Sci Technol. https://doi.org/10.1021/acs.est.4c14013.
[91] Lähteenmäki-Uutela, A., Rahikainen, M., Camarena-Gómez, M.T., Piiparinen, J., Spilling, K., Yang, B., 2021. European union legislation on macroalgae products. Aquac Int 29 (2), 487–509. https://doi.org/10.1007/S10499-020-00633-X/TABLES/1.
[92] Beiras, R., Fernández, N., Bellas, J., Besada, V., González-Quijano, A., Nunes, T., 2003. Integrative assessment of marine pollution in galician estuaries using sediment chemistry, mussel bioaccumulation, and embryo-larval toxicity bioassays. Chemosphere 52 (7), 1209–1224. https://doi.org/10.1016/S0045-6535(03)00364-3.
[93] Álvarez-Iglesias, P., Rubio, B., Millos, J., 2012. Isotopic identification of natural vs. Anthropogenic lead sources in marine sediments from the inner Ría de Vigo (NW Spain). Sci Total Environ 437, 22–35. https://doi.org/10.1016/J.SCITOTENV.2012.07.063.
[94] Billard, E., Daguin, C., Pearson, G., Serrão, E., Engel, C., Valero, M., 2005. Genetic isolation between three closely related taxa: fucus vesiculosus, F. Spiralis, and F. ceranoides (Phaophyceae). J Phycol 41 (4), 900–905. https://doi.org/10.1111/j.0022-3646.2005.04221.x.
[95] Neiva, J., Pearson, G.A., Valero, M., Serrão, E.A., 2012. Fine-scale genetic breaks driven by historical range dynamics and ongoing density-barrier effects in the Estuarine seaweed fucus ceranoides L. BMC Evol Biol 12 (1), 1–16. https://doi.org/10.1186/1471-2148-12-78/FIGURES/5.
[96] Garha, N.S., 2022. From decarbonization to depopulation: an emerging challenge for the carbon-intensive regions under the energy transition in Spain. Sustainability 14 (22), 14786. https://doi.org/10.3390/SU142214786.
[97] Council Directive. *Urban Wastewater Treatment Directive* (*91/271/EEC*); 1991.
[98] European Parliament and Council. *Directive 2000/60/EC Water Framework Directive*; 2000. ⟨https://eur-lex.europa.eu/eli/dir/2000/60/oj⟩ (accessed 2024-10-06).
[99] European Environment Agency. *Marine Strategy Framework Directive 2008/56/EC*; 2008. ⟨https://www.eea.europa.eu/policy-documents/2008-56-ec⟩.
[100] Vázquez-Arias, A., Pacín, C., Ares, Á., Fernández, J.Á., Aboal, J.R., 2023. Do we know the cellular location of heavy metals in seaweed? An up-to-date review of the techniques. Sci Total Environ 856 (September 2022). https://doi.org/10.1016/j.scitotenv.2022.159215.
[101] Bonachea, J., Remondo, J., Rivas, V., 2024. Estuaries in Northern Spain: an analysis of their sedimentation rates. Sustainability 16 (16), 6856. https://doi.org/10.3390/SU16166856.
[102] Perez-Arlucea, M., Mendez, G., Clemente, F., Nombela, M., Rubio, B., Filgueira, M., 2005. Hydrology, sediment yield, erosion and sedimentation rates in the estuarine environment of the Ria de Vigo, Galicia, Spain. J Mar Syst 54 (1–4), 209–226. https://doi.org/10.1016/J.JMARSYS.2004.07.013.
[103] Nathaniel, S.P., 2021. Ecological footprint and human well-being nexus: accounting for broad-based financial development, globalization, and natural resources in the Next-11 countries. Future Bus J 7 (1), 1–18. https://doi.org/10.1186/S43093-021-00071-Y.
[104] *Electronic waste (e-waste)*. ⟨https://www.who.int/news-room/fact-sheets/detail/electronic-waste-%28e-waste%29?utm_source=chatgpt.com⟩ (accessed 2025-01-14).
[105] Brooks, H.L., Miner, K.R., Kreutz, K.J., Winski, D.A., 2025. A global review of long-range transported lead concentration and isotopic ratio records in snow and ice. Environ Sci Process Impacts 27 (4), 878–891. https://doi.org/10.1039/D4EM00526K.
[106] Rusiecka, D., Gledhill, M., Milne, A., Achterberg, E.P., Annett, A.L., Atkinson, S., Birchill, A., Karstensen, J., Lohan, M., Mariez, C., Middag, R., Rolison, J.M., Tanhua, T., Ussher, S., Connelly, D., 2018. Anthropogenic signatures of lead in the Northeast Atlantic. Geophys Res Lett 45 (6), 2734–2743. https://doi.org/10.1002/2017GL076825.
[107] Bryan, G., Langston, W., Hummerstone, L.G., Burt, G.R., 1985. A guide to the assessment of heavy metal contamination in estuaries using biological indicators. Mar Biol Assoc 4, 92.
[108] Bryan, G.W., 1983. Brown seaweed, fucus vesiculosus, and the gastropod, littorina littoralis, as indicators of trace-metal availability in estuaries. Sci Total Environ 28 (1–3), 91–104. https://doi.org/10.1016/S0048-9697(83)80010-2.
[109] Barnett, B.E., Ashcroft, C.R., 1985. Heavy metals in fucus vesiculosus in the humber estuary. Environ Pollut Ser B Chem Phys 9 (3), 193–213. https://doi.org/10.1016/0143-148X(85)90033-3.
[110] García-Seoane, R., Fernández, J.A., Varela, Z., Real, C., Boquete, M.T., Aboal, J. R., 2019. Sampling optimization for biomonitoring metal contamination with marine macroalgae. Environ Pollut 255, 113349. https://doi.org/10.1016/j.envpol.2019.113349.
[111] Caldeira, K., Wickett, M.E., 2003. Anthropogenic carbon and ocean PH, 365–365 Nature 425 (6956). https://doi.org/10.1038/425365a.
[112] Millero, F.J., Woosley, R., Ditrolio, B., Waters, J., 2009. Effect of ocean acidification on the speciation of metals in seawater. Oceanography 22 (4), 72–85. https://doi.org/10.5670/OCEANOG.2009.98.
[113] Vignier, J., Champeau, O., Atalah, J., South, P., McDougall, D., Jeffs, A., Blackwell, D., Tremblay, L.A., Rolton, A., 2025. Land-derived metals impact the survival and settlement of larval mussels. Environ Pollut 367, 125675. https://doi.org/10.1016/J.ENVPOL.2025.125675.
[114] Lan, W.R., Huang, X.G., Lin, L. xiu, Li, S.X., Liu, F.J., 2020. Thermal discharge influences the bioaccumulation and bioavailability of metals in oysters: implications of ocean warming. Environ Pollut 259, 113821. https://doi.org/10.1016/J.ENVPOL.2019.113821.
[115] Vázquez-Arias, A., Boquete, M.T., Fernández, J.Á., Aboal, J.R., 2025. Assessing the effectiveness of seaweed transplants in reflecting seawater pollution levels. Environ Pollut 377, 126456. https://doi.org/10.1016/j.envpol.2025.126456.
[116] Schultz, J., Berry Gobler, D.L., Young, C.S., Perez, A., Doall, M.H., Gobler, C.J., 2024. Ocean acidification significantly alters the trace element content of the Kelp, Saccharina Latissima. Mar Pollut Bull 202, 116289. https://doi.org/10.1016/J.MARPOLBUL.2024.116289.
[117] Maharana, D., Jena, K., Pise, N.M., Jagtap, T.G., 2010. Assessment of oxidative stress indices in a marine macro brown alga padina tetrastromatica (hauck) from comparable polluted coastal regions of the Arabian Sea, West Coast of India. J Environ Sci 22 (9), 1413–1417. https://doi.org/10.1016/S1001-0742(09)60268-0.
[118] Andrade, L.R., Leal, R.N., Noseda, M., Duarte, M.E.R., Pereira, M.S., Mourão, P.A. S., Farina, M., Amado Filho, G.M., 2010. Brown algae overproduce cell wall polysaccharides as a protection mechanism against the heavy metal toxicity. Mar Pollut Bull 60 (9), 1482–1488. https://doi.org/10.1016/j.marpolbul.2010.05.004.
[119] García-Seoane, R.; Richards, C.L.; Aboal, J.R.; Fernández, J.Á.; Schmid, M.W.; Boquete, M.T. A Field Study of the Molecular Response of Brown Macroalgae to Heavy Metal Exposure: An (Epi)Genetic Approach. https://doi.org/10.2139/SSRN.4896934.
[120] European Environment Agency. *Heavy metal emissions in Europe*. ⟨https://www.eea.europa.eu/data-and-maps/indicators/eea32-heavy-metal-hm-emissions-2/assessment⟩. croalgae to Heavy Metal Exposure: An (Epi)Genetic Approach. https://doi.org/10.2139/SSRN.4896934.